

## ■ Artificial Nucleoside

## Silver(I) Coordination in Silver(I)-Mediated Homo Base Pairs of 6-Pyrazolypurine in DNA Duplexes Involves the Watson–Crick Edge

Daniela Escher and Jens Müller\*<sup>[a]</sup>*Dedicated to Professor Stephen J. Lippard on the occasion of this 80th birthday*

**Abstract:** DNA duplexes comprising 6-(1*H*-pyrazol-1-yl)-9*H*-purine (6PP), 1-deaza-6PP (<sup>10</sup>6PP), 7-deaza-6PP (<sup>7D</sup>6PP) and 1,7-dideaza-6PP (<sup>1,7D</sup>6PP) 2'-deoxyribonucleosides, respectively, were investigated towards their ability to form metal-mediated base pairs in the presence of Ag<sup>I</sup>. In 6PP and <sup>7D</sup>6PP, the Ag<sup>I</sup> ion can coordinate to the nucleobase via the endocyclic N1 nitrogen atom, that is, via the Watson–Crick edge. In contrast, this nitrogen atom is not available in <sup>10</sup>6PP and <sup>1,7D</sup>6PP, so that in <sup>10</sup>6PP an Ag<sup>I</sup> coordination is only pos-

sible via the Hoogsteen edge (N7). Reference duplexes with either adenine:adenine mispairs or canonical adenine:thymine base pairs were used to investigate the impact of the pyrazolyl moiety on the Ag<sup>I</sup>-binding properties. To determine the thermal and structural duplex stabilities in the absence or presence of Ag<sup>I</sup>, all duplexes were examined by UV and circular dichroism spectroscopic studies. These investigations shed light on the question of whether N1- or N7-coordination is preferred in purine-based metal-mediated base pairs.

## Introduction

In 1963, a base pairing pattern for canonical nucleobases in double-stranded DNA was proposed that is different from the one originally put forward by Watson and Crick.<sup>[1]</sup> While Watson and Crick suggested the formation of base pairs via the N1 nitrogen atom of the purine bases in DNA,<sup>[1a]</sup> Hoogsteen crystallized a complex of 9-methyladenine and 1-methylthymine in which the N7 nitrogen atom of the adenine derivative was involved in the formation of the A:T base pair.<sup>[1b]</sup> Even though it is nowadays accepted that canonical base pairing occurs almost exclusively via the Watson–Crick edge in antiparallel-stranded DNA duplexes,<sup>[2]</sup> the Hoogsteen edge can be of relevance when artificial nucleosides are involved.<sup>[3]</sup> As artificial nucleobases are not restricted to the geometry and binding sites of their natural counterparts, formation of base pairs may involve hydrogen bonding,<sup>[4]</sup> hydrophobic interactions in combination with shape complementarity<sup>[5]</sup> or coordination of metal ions.<sup>[6]</sup> In the latter case, hydrogen bonds are formally replaced by coordinate bonds to metal ions resulting in the for-

mation of metal-mediated base pairs.<sup>[7]</sup> DNA duplexes comprising artificial ligand-derived nucleosides are typically destabilized in the absence of suitable transition metal ions compared to canonical DNA duplexes, because their arrangement of Lewis-basic donor sites is optimized for the formation of metal complexes rather than for hydrogen bonds.<sup>[7a,b]</sup> However, upon the addition of suitable metal ions, the melting temperature of these DNA duplexes increases, indicating a higher thermal stability due to the formation of metal-mediated base pairs.<sup>[8]</sup> The respective degree of stabilization depends on the chosen nucleobase and hence on the type of coordinating metal ion. Several applications have been put forward for DNA with metal-mediated base pairs, including metal-responsive structural and catalytic transformations,<sup>[9]</sup> sensors for metal ions or oligonucleotides,<sup>[10]</sup> modulation of the charge-transfer capabilities of DNA,<sup>[11]</sup> generation of metal nanoclusters,<sup>[12]</sup> and several more.<sup>[7a]</sup> While even the naturally occurring nucleobases are capable of forming metal-mediated base pairs,<sup>[13]</sup> the majority of published metal-mediated base pairs contains artificial nucleosides,<sup>[8]</sup> based on monodentate,<sup>[14]</sup> bidentate,<sup>[15]</sup> tridentate<sup>[16]</sup> or even tetradentate<sup>[17]</sup> ligands. Depending on the identity of the artificial nucleobase, up to three metal ions can be introduced into a single metal-mediated base pair.<sup>[18]</sup> Many of the artificial nucleobases are derivatives of purine and pyrimidine. In the context of this work, purine-derived ligands are of particular interest. Most of these derivatives bear an additional metal-binding entity at their C2 and/ or their C6 position,<sup>[3f,19]</sup> while others are guanine and adenine derivatives with formally exchanged N/C–H positions.<sup>[20]</sup>

6-(1*H*-Pyrazol-1-yl)-9*H*-purine (6PP) is an adenine-derived artificial nucleobase comprising a pyrazolyl moiety instead of the exocyclic amine group (Scheme 1), that is, bearing an addition-

[a] Dr. D. Escher, Prof. Dr. J. Müller  
Westfälische Wilhelms-Universität Münster  
Institut für Anorganische und Analytische Chemie  
Corrensstr. 30, 48149 Münster (Germany)  
E-mail: mueller.j@uni-muenster.de

Supporting information and the ORCID identification number(s) for the author(s) of this article can be found under:  
<https://doi.org/10.1002/chem.202002803>.

© 2020 The Authors. Published by Wiley-VCH GmbH. This is an open access article under the terms of Creative Commons Attribution NonCommercial-NoDerivs License, which permits use and distribution in any medium, provided the original work is properly cited, the use is non-commercial and no modifications or adaptations are made.

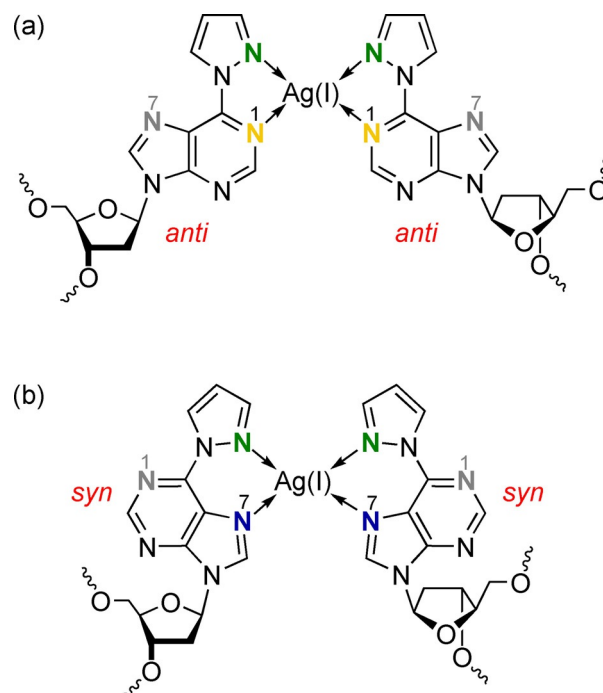


**Scheme 1.** The artificial nucleobase 6-(1H-pyrazol-1-yl)-9H-purine (6PP) including an atom-numbering scheme using the purine nomenclature. Metal-binding sites for the formation of metal-mediated base pairs are indicated in bold.

bind to the N7 atom.<sup>[22]</sup> Similarly, the N7 position was proposed as the most likely Cu<sup>II</sup>-binding site in oligonucleotides carrying an artificial nucleoside with a 6-(1H-3,5-dimethylpyrazol-1-yl)-9H-purine nucleobase.<sup>[19d]</sup> On the other hand, taking into consideration the reports on different geometries of the A:T pair in a DNA duplex (by Watson and Crick)<sup>[1a]</sup> and in a model nucleobase complex (by Hoogsteen),<sup>[1b]</sup> it is possible that the preferred binding mode of 6PP in a DNA duplex differs from that found in the <sup>Me</sup>6PP-M<sup>Me</sup>6PP model nucleobase complexes (M = Ag<sup>I</sup>, Cu<sup>II</sup>).<sup>[19f]</sup>

To identify the Ag<sup>I</sup>-binding pattern in a 6PP-Ag<sup>I</sup>-6PP base pair inside a DNA duplex, a selection of 6PP-derived 2'-deoxyribonucleosides was incorporated into antiparallel-stranded DNA duplexes bearing three adjacent artificial homo base pairs in the center of the duplex. In addition to the 6PP deoxyribonucleoside, this set includes the 1-deaza-6PP (<sup>1D</sup>6PP), 7-deaza-6PP (<sup>7D</sup>6PP) and 1,7-dideaza-6PP (<sup>1,7D</sup>6PP) deoxyribonucleosides. While the absence of the N7 nitrogen atom in <sup>7D</sup>6PP should favor Ag<sup>I</sup> coordination via the Watson-Crick edge (i.e. via N1) (Scheme 2a), <sup>1D</sup>6PP lacks the N1 nitrogen atom but possesses an N7 nitrogen atom, allowing an Ag<sup>I</sup>-mediated base pair formation via the Hoogsteen edge (Scheme 2b). It is important to note that for metal-mediated base pair formation via the Watson-Crick edge the nucleosides retain their normal *anti* orientation of nucleobase and deoxyribose moiety (Scheme 2a). In contrast, the less common *syn* orientation must be adopted to enable metal-mediated base pairing via the Hoogsteen edge inside an antiparallel-stranded double helix (Scheme 2b). Nevertheless, several examples have been reported in which such a *syn* orientation is present in metal-mediated base pairs.<sup>[3a,f,13b]</sup> In addition to duplexes bearing 6PP, <sup>1D</sup>6PP or <sup>7D</sup>6PP, DNA duplexes comprising either <sup>1,7D</sup>6PP or A deoxyribonucleosides were studied to determine the relevance of the pyrazolyl moiety on Ag<sup>I</sup>-mediated base pair formation. All DNA duplexes were investigated by temperature-dependent UV spectroscopy and circular dichroism (CD) spectroscopy to compare their Ag<sup>I</sup>-binding behavior and its influence on thermal stability and duplex structure.

al metal-binding moiety at its N6 position. Because of the free rotatability around the C6-N1\* bond, the nitrogen atom of the pyrazolyl substituent can either face the Watson-Crick or the Hoogsteen edge. Prior studies of metal complexes involving the N9-methylated 6PP model nucleobase <sup>Me</sup>6PP and either Ag<sup>I</sup> or Cu<sup>II</sup> have shown that coordination via the Hoogsteen edge (N7) and the pyrazole N2\* nitrogen atom is favored in the solid state.<sup>[21]</sup> This is in good agreement with earlier studies on the canonical purine bases, indicating that metal ions preferentially

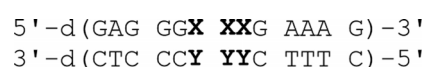


**Scheme 2.** Possible binding patterns of 6PP-Ag<sup>I</sup>-6PP base pairs via the Watson-Crick edge (a) or the Hoogsteen edge (b). The nitrogen atoms not involved in Ag<sup>I</sup> binding are depicted in grey to emphasize the expected pattern for a DNA duplex with either <sup>7D</sup>6PP or <sup>1D</sup>6PP nucleosides. The terms *anti* and *syn* refer to the relative orientation of nucleobase and deoxyribose.

## Results and Discussion

The general sequence of the DNA duplexes under investigation is depicted in Scheme 3. Six duplexes were selected, including either homo base pairs (X = Y) of 6PP (I), <sup>1D</sup>6PP (II), <sup>7D</sup>6PP (III), <sup>1,7D</sup>6PP (IV) and adenine (V) or central A:T pairs (VI), serving as a reference. All duplexes contain three consecutive metal-binding sites because initial tests had indicated that these sequences can be significantly stabilized by the addition of Ag<sup>I</sup>.

To evaluate the thermal stability of the DNA duplexes, their melting temperatures were determined UV-spectroscopically in the absence of Ag<sup>I</sup> and after the addition of up to 6 μM Ag<sup>I</sup>, corresponding to two Ag<sup>I</sup> ions per artificial base pair in duplexes I–V. The Ag<sup>I</sup> concentration was increased in steps of 1 μM between 0 μM and 3 μM of Ag<sup>I</sup> to evaluate possible differences in binding affinity. An exemplary melting curve is given in Figure 1, showing the data for duplex I. The melting curves of all other duplexes are shown in the Supporting information (Figure S2). Melting temperatures ( $T_m$ ) were derived from each melting curve and plotted against the respective concentration of Ag<sup>I</sup> (Figure 2). The  $T_m$  values for 0 equiv (0 μM), 1 equiv (3 μM) and 2 equiv (6 μM) of Ag<sup>I</sup> as well as the increase in  $T_m$  ( $\Delta T_m$ ) between 0 and 1 equiv of Ag<sup>I</sup> are summarized in Table 1.



**Scheme 3.** DNA duplexes investigated in this study. For definition of X and Y, see text.

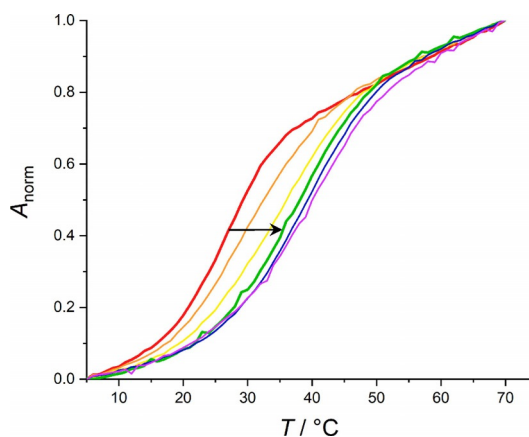


**Figure 1.** Melting curves of DNA duplex I with three central 6PP:6PP pairs in the presence of 0  $\mu\text{M}$  (red), 1  $\mu\text{M}$  (orange), 2  $\mu\text{M}$  (yellow), 3  $\mu\text{M}$  (green), 4  $\mu\text{M}$  (blue) and 6  $\mu\text{M}$  (purple) of  $\text{Ag}^+$ . 3  $\mu\text{M}$   $\text{Ag}^+$   $\hat{=}$  1 equiv of  $\text{Ag}^+$  with respect to the number of 6PP:6PP pairs. Experimental conditions: 1  $\mu\text{M}$  DNA duplex, 5 mM MOPS buffer (pH 6.8), 150 mM  $\text{NaClO}_4$ .

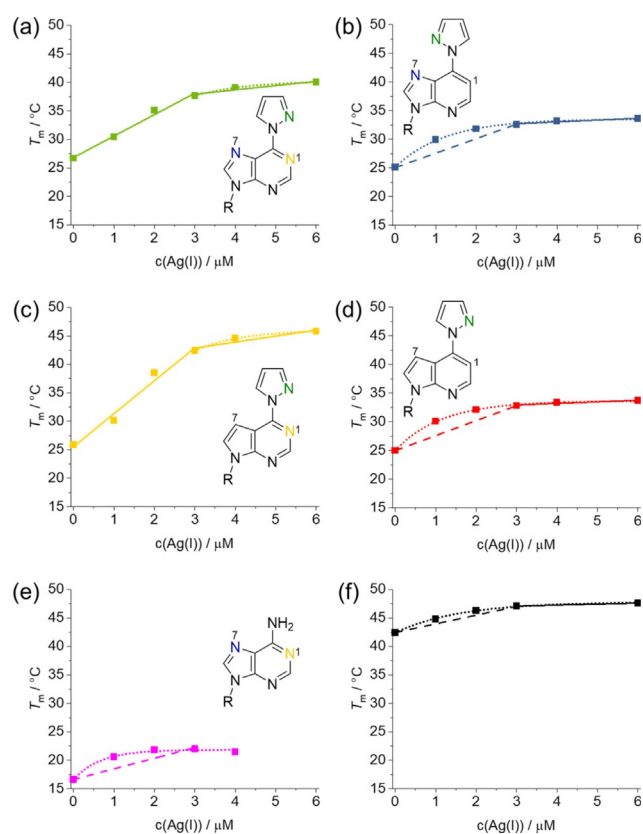


**Figure 2.** Plot of the melting temperatures of duplexes I (a), II (b), III (c), IV (d), V (e) and VI (f) with linear fit (solid line), hypothetical linear fit between 0  $\mu\text{M}$  and 3  $\mu\text{M}$   $\text{Ag}^+$  (broken line) or asymptotic fit (dotted line). The hypothetical linear fit indicates the anticipated course of data points for three high-affinity binding sites. The asymptotic fit resembles the course of data points for an unspecified number of low-affinity binding sites. 3  $\mu\text{M}$   $\text{Ag}^+$   $\hat{=}$  1 equiv of  $\text{Ag}^+$  corresponds to the concentration required to introduce one  $\text{Ag}^+$  ion into each designated  $\text{Ag}^+$ -binding site. For clarity, the respective artificial nucleobase is shown, too. In Figure 2 f, no nucleobase is indicated, because this is the reference measurement with three central A:T base pairs. Experimental conditions: 1  $\mu\text{M}$  DNA duplex, 5 mM MOPS buffer (pH 6.8), 150 mM  $\text{NaClO}_4$ .

Table 1. Melting temperatures $T_m$ for duplexes I–VI. <sup>[a]</sup>				
Duplex	$T_m$ [°C] 0 $\mu\text{M}$ $\text{Ag}^+$	$T_m$ [°C] 3 $\mu\text{M}$ $\text{Ag}^+$	$T_m$ [°C] 6 $\mu\text{M}$ $\text{Ag}^+$	$\Delta T_m$ [°C] 0 $\rightarrow$ 3 $\mu\text{M}$ $\text{Ag}^+$
I	26.7(1)	37.7(4)	40.1(4)	11.0(4)
II	25.1(2)	32.6(3)	33.6(5)	7.5(4)
III	25.9(1)	42.4(5)	46.0(8)	16.5(5)
IV	25.0(2)	32.8(3)	33.7(6)	7.8(4)
V	16.6(2)	22.0(4)	–	5.4(4)
VI	42.4(1)	47.1(1)	47.6(1)	4.7(1)

[a] Standard deviation given in parenthesis. Values obtained by fitting the derivative of the melting curve with a Gauss function, considering a confidence interval of 95% (for  $T_m$ ), or by using error propagation (for  $\Delta T_m$ ).

As expected, duplex VI bearing only canonical base pairs reveals the highest melting temperature with a  $T_m$  of 42.4 °C in the absence of  $\text{Ag}^+$ . Interestingly, all duplexes comprising 6PP-derived nucleosides (I–IV) have almost the same thermal stability in the absence of  $\text{Ag}^+$  ( $T_m = 25.0$ – $26.7$  °C), indicating that the absence or presence of the endocyclic nitrogen atoms N1 and N7 plays a minor role in the stabilization of the DNA duplex. However, the absence of the pyrazolyl moiety has a significant impact on stability. Duplex V with its central A:A mispairs is further destabilized by 10 °C compared to duplex I, even though both 6PP (duplex I) and adenine (duplex V) contain N1 and N7 atoms. Apparently, the aromatic pyrazole ring introduces additional stability. Upon the addition of 3  $\mu\text{M}$   $\text{Ag}^+$ , all duplexes are thermally stabilized, including reference duplex VI. As this duplex does not contain any designated  $\text{Ag}^+$  binding sites,  $\text{Ag}^+$  may interact with the donor atoms of the natural nucleobases,<sup>[13b,20e]</sup> leading to a slightly increased melting temperature ( $\Delta T_m = 4.7$  °C). The same behavior is also observed for duplex V ( $\Delta T_m = 5.4$  °C). In both cases, the plot of melting temperature vs. amount of  $\text{Ag}^+$  (Figure 2e,f) shows an asymptotic behavior, indicating a small binding constant.<sup>[23]</sup>

Interestingly, it is possible to distinguish between duplexes I–IV based on the plots shown in Figure 2 with respect to the absence (duplexes II (<sup>1D</sup>6PP, Figure 2b) and IV (<sup>1,7D</sup>6PP, Figure 2d)) or presence (duplexes I (6PP, Figure 2a) and III (<sup>7D</sup>6PP, Figure 2c)) of an endocyclic N1 atom. For the former, not only the differences in thermal stabilization upon  $\text{Ag}^+$ -binding are the same (II: 7.5 °C; IV: 7.8 °C), but also the absolute melting temperature in the absence of  $\text{Ag}^+$  (II: 25.1 °C; IV: 25.0 °C) and in the presence of 3  $\mu\text{M}$   $\text{Ag}^+$  (II: 32.6 °C; IV: 32.8 °C). As the 6PP-derived nucleosides in duplexes II and IV do not contain any N1 nitrogen atoms, possible  $\text{Ag}^+$ -mediated base pairs cannot involve their Watson–Crick edge. Nevertheless, their pyrazolyl moiety is likely to play a role in coordinating the  $\text{Ag}^+$  ions, because the increase in  $T_m$  upon the addition of  $\text{Ag}^+$  is slightly higher for II and IV compared to V and VI. For these four duplexes (II, IV, V and VI), the plots of melting temperature vs. amount of  $\text{Ag}^+$  can be fitted best in an asymptotic manner, which is representative of a low binding affinity. However, the increase in  $T_m$  upon binding of  $\text{Ag}^+$  is larger for those duplexes containing an artificial nucleobase with the pyrazolyl moiety (II, IV), indicating the relevance of this substituent in  $\text{Ag}^+$  binding. Here, a potential low-affinity binding site could be

provided by two consecutive artificial base pairs coordinating one  $\text{Ag}^{\text{I}}$  ion in-between them. This possibility is currently being explored in our laboratory, using optimized oligonucleotide sequences.

The largest increase in thermal stability is observed for duplex III ( $\Delta T_m = 16.5^\circ\text{C}$ ), and duplex I is also significantly stabilized ( $\Delta T_m = 11.0^\circ\text{C}$ ). The plots of  $T_m$  vs. amount of  $\text{Ag}^{\text{I}}$  are quite similar for these two duplexes (Figure 2a, c). Here, the melting temperature increases linearly with increasing concentrations of  $\text{Ag}^{\text{I}}$  up to the addition of  $3\ \mu\text{M}$   $\text{Ag}^{\text{I}}$ , which corresponds to the presence of one  $\text{Ag}^{\text{I}}$  ion per designated  $\text{Ag}^{\text{I}}$ -mediated base pair. Excess  $\text{Ag}^{\text{I}}$  leads to a much smaller additional increase in  $T_m$ . In combination, these observations clearly indicate the formation of stable  $\text{Ag}^{\text{I}}$ -mediated base pairs. Moreover, as duplex III contains  ${}^{\text{7D}}$ 6PP moieties lacking the N7 atom, these  $\text{Ag}^{\text{I}}$ -mediated base pairs must involve the Watson–Crick edge with its N1 donor site. Interestingly, the thermal stability of duplex III bearing  ${}^{\text{7D}}$ 6PP significantly exceeds that of duplex I with 6PP once the  $\text{Ag}^{\text{I}}$ -mediated base pairs are formed. Different explanations are feasible here: The larger stabilization could be due to different electronic properties of  ${}^{\text{7D}}$ 6PP compared to 6PP, leading to a higher affinity towards  $\text{Ag}^{\text{I}}$  ions. Alternatively, the  ${}^{\text{7D}}$ 6PP nucleosides may fit better into the base stack compared to 6PP. However, a final conclusion cannot be drawn, because a determination of the  $\text{p}K_{\text{a}}$  values by pD-dependent  ${}^1\text{H}$  NMR spectroscopy does not indicate significantly different basicities of the 6PP and  ${}^{\text{7D}}$ 6PP deoxyribonucleosides (Figure S1, Supporting information). Similarly, the second possible explanation is unlikely, considering that canonical DNA with A:T pairs was reported to be more stable than DNA with  ${}^{\text{7D}}$ A:T base pairs.<sup>[24]</sup>

The addition of more than one equivalent of  $\text{Ag}^{\text{I}}$  ( $3\ \mu\text{M}$ ) results in a minor additional increase in  $T_m$  for all six duplexes when compared to the stabilizing effect of the first equivalent of  $\text{Ag}^{\text{I}}$ . For duplexes II, IV and VI, this additional increase amounts to ca.  $1^\circ\text{C}$ , while it is slightly higher for duplexes I ( $2.4^\circ\text{C}$ ) and III ( $3.6^\circ\text{C}$ ). Similar to what is observed for the interaction of canonical duplexes with  $\text{Ag}^{\text{I}}$ , it is likely that once all designated  $\text{Ag}^{\text{I}}$ -binding sites are saturated with  $\text{Ag}^{\text{I}}$ , additional interactions with the remaining natural nucleobases occur. This leads to the additional small increase in  $T_m$  observed as an asymptotic change of  $T_m$  between  $3\ \mu\text{M}$  and  $6\ \mu\text{M}$   $\text{Ag}^{\text{I}}$  (Figure 2). For duplex V, no melting temperature could be determined in the presence of  $6\ \mu\text{M}$   $\text{Ag}^{\text{I}}$  because no sigmoid melting curve was observed (Figure S2e, Supporting information).

Besides the thermal stability of the DNA duplexes, a possible change of their structure upon the addition of  $\text{Ag}^{\text{I}}$  was investigated by CD spectroscopy. The CD spectra for duplexes I–VI are depicted in Figure 3. At first glance, the spectra for duplexes I and II, III and IV or V and VI look similar in the absence of  $\text{Ag}^{\text{I}}$ . This does not only reflect the helical structure but also the different UV absorbance resulting from the presence of different artificial deoxyribonucleosides. The UV spectra for duplexes I–VI (Figure S3, Supporting information) confirm the presence of additional absorbance maxima at 305 nm (for I and II) and ca. 325 nm (for III and IV) that can be assigned to

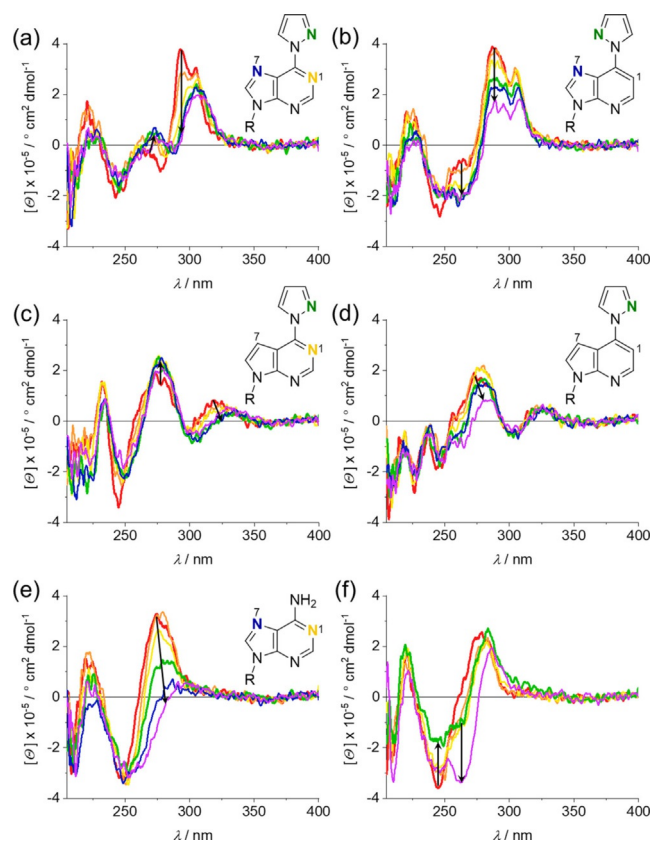


**Figure 3.** CD spectra of duplexes I (a), II (b), III (c), IV (d), V (e) and VI (f) in the presence of  $0\ \mu\text{M}$  (red),  $1\ \mu\text{M}$  (orange),  $2\ \mu\text{M}$  (yellow),  $3\ \mu\text{M}$  (green),  $4\ \mu\text{M}$  (blue) and  $6\ \mu\text{M}$  (purple)  $\text{Ag}^{\text{I}}$ . Important changes are highlighted by arrows.  $3\ \mu\text{M}$   $\text{Ag}^{\text{I}} \triangleq 1$  equiv of  $\text{Ag}^{\text{I}}$  with respect to the number of mismatches. For clarity, the respective artificial nucleobase is shown, too. In Figure 2f, no nucleobase is indicated, because this is the reference measurement with three central A:T base pairs. Experimental conditions:  $1\ \mu\text{M}$  DNA duplex,  $5\ \text{mM}$  MOPS buffer (pH 6.8),  $150\ \text{mM}$   $\text{NaClO}_4$ .

the pyrazolyl moiety as seen before for other C6-substituted purines.<sup>[19g]</sup>

In analogy to the trends found for  $T_m$ , the CD spectrum of duplex I (Figure 3a) changes significantly up to the addition of  $3\ \mu\text{M}$   $\text{Ag}^{\text{I}}$ . Already in the presence of only  $1\ \mu\text{M}$   $\text{Ag}^{\text{I}}$ , the small maximum at 265 nm shifts to 272 nm and increases simultaneously. The maximum at 293 nm becomes a shoulder in the presence of  $2\ \mu\text{M}$   $\text{Ag}^{\text{I}}$ , while the maximum at 305 nm assigned to the pyrazolyl moiety decreases steadily until  $3\ \mu\text{M}$  of  $\text{Ag}^{\text{I}}$  are present in solution, only to remain unchanged thereafter. All this indicates that three  $\text{Ag}^{\text{I}}$  ions are coordinated per duplex, causing a structural change due to the formation of three  $\text{Ag}^{\text{I}}$ -mediated base pairs. Once all mismatches are saturated, the helical structure does not change any further. For duplex II (Figure 3b), the same changes of the maximum at 305 nm are observed, but in contrast to duplex I, excess  $\text{Ag}^{\text{I}}$  influences the DNA structure further, leading to a continued decrease of this maximum. The same trend is followed by the maximum at 288 nm, but in contrast to the related maximum of duplex I (at 293 nm), it does not disappear. Furthermore, the negative maximum at 260 nm in the CD spectrum of duplex II steadily changes to become a minimum, while the respective maxi-

imum of duplex I at 265 nm increases and shifts to higher wavelengths as mentioned before. The fact that the CD spectra of duplexes I and II change differently upon the addition of Ag<sup>I</sup> suggests that different Ag<sup>I</sup>-binding modes are adopted by the duplexes. The <sup>1D</sup>6PP:<sup>1D</sup>6PP pairs in duplex II can bind the Ag<sup>I</sup> ions only via the Hoogsteen edge, so that a binding of Ag<sup>I</sup> via the Watson–Crick edge appears likely for the 6PP:6PP pairs in duplex I.

CD spectra of duplex III (containing <sup>7D</sup>6PP, Figure 3c) show only minor changes upon the addition of up to one equivalent of Ag<sup>I</sup> and further addition does not affect the duplex structure anymore. Upon the addition of 1 μM Ag<sup>I</sup>, the minimum at 246 nm decreases and the maximum at 276 nm becomes slightly more intense while the local maximum assigned to the presence of the pyrazolyl substituent shifts from 320 nm to 330 nm. As such a shift is not observed for the corresponding maximum in the CD spectrum of duplex IV (containing <sup>1,7D</sup>6PP), it can be assumed that the formation of Ag<sup>I</sup>-mediated base pairs involving the N1 nitrogen atom leads either to a structural change of the duplex or to an electronic change of the nucleobases. Furthermore, the direction of the change of the maximum at 276 nm of duplex III is perfectly in line with that of duplex I, confirming once more that duplexes with either 6PP:6PP or <sup>7D</sup>6PP:<sup>7D</sup>6PP pairs behave similarly upon the addition of Ag<sup>I</sup>.

Even if the melting temperatures of duplexes V and VI are affected only slightly by the addition of Ag<sup>I</sup>, the concomitant structural changes are highly significant. The maximum in the CD spectrum of duplex V at 275 nm decreases continuously with increasing Ag<sup>I</sup> concentration. It is worth mentioning that the *T<sub>m</sub>* plot reaches a plateau in the presence of 2 μM Ag<sup>I</sup>, while major changes in the CD spectra continue to take place even upon the addition of more than 2 μM Ag<sup>I</sup>. The significantly affected structure in the presence of 6 μM Ag<sup>I</sup> also explains why no sigmoid melting curve was observed anymore under these conditions. In contrast to all other duplexes, duplex VI bearing only canonical base pairs shows significant yet no continuous changes in the presence of increasing amounts of Ag<sup>I</sup>. Even though the *T<sub>m</sub>* plot suggests a stable, almost unaltered duplex structure in the absence and presence of Ag<sup>I</sup>, the CD experiments refute this assumption. After the addition of 1 μM Ag<sup>I</sup>, the negative Cotton effect at 245 nm becomes less intense and the maximum at 278 nm is shifted slightly to higher wavelengths. While the presence of 2 μM Ag<sup>I</sup> does not induce any further changes to the CD spectrum, the addition of 3 μM Ag<sup>I</sup> leads to a further increase of the ellipticity at 245 nm along with a broadening of the minimum and the maximum. Upon the addition of more than 3 μM Ag<sup>I</sup>, massive changes in the CD spectrum are observed, whereas the thermal stability studies indicate almost no change ( $\Delta T_m = 0.5^\circ\text{C}$ ). The broad minimum now splits into two intensive minima and the positive Cotton effect decreases in intensity. These changes clearly point out that melting temperatures and thus thermal stabilities alone do not allow the prediction of the duplex integrity. A possible explanation for the large CD spectroscopic changes is the coordination of Ag<sup>I</sup> to the N7 position of the purine nucleobases, as previously proposed in other studies.<sup>[20e]</sup> Interest-

ingly, oligonucleotides in which all purine residues are replaced by 7-deazapurine moieties show a completely different behaviour,<sup>[20a]</sup> supporting the assumption that the CD spectroscopic changes observed for duplexes V and VI involve a coordination of Ag<sup>I</sup> to N7.

## Conclusions

By using a set of DNA duplexes with artificial (deaza)-6-pyrazolylpurine-derived 2'-deoxyribonucleosides, we could show that the affinity towards Ag<sup>I</sup> varies depending on the provided binding sites. Strongly stabilizing Ag<sup>I</sup>-mediated base pairs are preferentially formed via the Watson–Crick edge (coordination via N1), as observed for the duplexes with 6PP and <sup>7D</sup>6PP (I and III). In these cases, metal-mediated base pair formation is accompanied by a structural change of the duplex, but the presence of excess Ag<sup>I</sup> does not further affect the helical structure. Artificial nucleosides lacking the N1 atom as a potential metal-binding site (<sup>1D</sup>6PP and <sup>1,7D</sup>6PP, duplexes II and IV) form less stabilizing metal-mediated base pairs. Moreover, the binding affinity is significantly decreased in these cases. Nevertheless, the presence of a pyrazolyl moiety increases the Ag<sup>I</sup> affinity of the nucleobase compared to that of adenine, as Ag<sup>I</sup> may still interact with the N2\* nitrogen atom of the appended pyrazole. These duplexes therefore show a slight increase in their melting temperature in the presence of one equivalent of Ag<sup>I</sup> (3 μM), accompanied by changes in the helical structure. In contrast to duplexes I and III, excess Ag<sup>I</sup> induces further structural changes in duplexes II and IV. Furthermore, duplexes with A:A mismatches or canonical A:T pairs as their central base pairs were investigated. Although their thermal stability is barely affected by the presence of Ag<sup>I</sup>, structural changes of the DNA helices are considerably strong. These observations emphasize that not only the presence of the N1 nitrogen atom but the synergy of the latter and the pyrazolyl moiety leads to the site-specific incorporation of Ag<sup>I</sup> ions to form DNA duplexes with strongly stabilizing Ag<sup>I</sup>-mediated base pairs. In contrast to what had previously been suggested based on single-molecule X-ray diffraction analysis of Ag<sup>I</sup> complexes of the corresponding model nucleobases, 6PP seems to prefer Ag<sup>I</sup>-binding via its Watson–Crick edge in Ag<sup>I</sup>-mediated homo base pairs in a DNA duplex.

## Experimental Section

Oligonucleotides used for duplexes I–VI were synthesized and purified as described previously.<sup>[25]</sup> Phosphoramidites of the natural nucleobases were purchased (Glen Research) and artificial phosphoramidites were synthesized similar to the procedure published before for the 6PP phosphoramidite (see Supporting information for details).<sup>[7]</sup> The desalted oligonucleotides were characterized by MALDI-TOF mass spectrometry (see Supporting information, Figure S4, for details; duplex I, strand 1: calcd for [M+H]<sup>+</sup>: 4258.8 Da; found: 4258.8 Da; duplex I, strand 2: calcd for [M+H]<sup>+</sup>: 3982.7 Da; found: 3982.6 Da; duplex II, strand 1: calcd for [M+H]<sup>+</sup>: 4255.8 Da; found: 4256.0 Da; duplex II, strand 2: calcd for [M+H]<sup>+</sup>: 3981.7 Da; found: 3982.2 Da; duplex III, strand 1: calcd for [M+H]<sup>+</sup>: 4258.8 Da; found: 4258.4 Da; duplex III, strand 2: calcd for [M+H]<sup>+</sup>:

3980.7 Da; found: 3981.0 Da; duplex IV, strand 1: calcd for  $[M+H]^+$ : 4251.8 Da; found: 4251.8 Da; duplex IV, strand 2: calcd for  $[M+H]^+$ : 3975.7 Da; found: 3975.3 Da; duplex V/VI, strand 1: calcd for  $[M+H]^+$ : 4106.8 Da; found: 4106.8 Da; duplex V, strand 2: calcd for  $[M+H]^+$ : 3831.7 Da; found: 3831.1 Da; duplex VI, strand 2: calcd for  $[M+H]^+$ : 3803.7 Da; found: 3804.1 Da. Oligonucleotide concentrations were determined by UV spectroscopy using the following molar extinction coefficients for the artificial nucleosides:  $\epsilon_{260}(\text{6PP}) = 4.8 \text{ cm}^2 \mu\text{mol}^{-1}$ ,  $\epsilon_{260}(\text{10}^6\text{PP}) = 8.6 \text{ cm}^2 \mu\text{mol}^{-1}$ ,  $\epsilon_{260}(\text{7D}^6\text{PP}) = 7.0 \text{ cm}^2 \mu\text{mol}^{-1}$ ,  $\epsilon_{260}(\text{1,7D}^6\text{PP}) = 2.5 \text{ cm}^2 \mu\text{mol}^{-1}$ . UV experiments were carried out on a CARY 100 Bio UV spectrometer (Agilent) and CD studies were performed using a J-815 CD spectrometer (Jasco). All measurements were done in a quartz cuvette with 1 cm diameter at 5 °C. In case of the melting studies, absorbance at 260 nm was recorded continuously while heating from 5 °C to 70 °C. The melting temperature was determined from a Gaussian fit of the first derivative of the melting curve. The probed DNA solutions consist of 1  $\mu\text{M}$  DNA duplex, 5 mM MOPS buffer (pH 6.8) and 150 mM  $\text{NaClO}_4$ .  $\text{AgNO}_3$  was used for titration experiments.

## Acknowledgements

We gratefully acknowledge the DFG (IRTG 2027, SFB 858) for funding. Open access funding enabled and organized by Projekt DEAL.

## Conflict of interest

The authors declare no conflict of interest.

**Keywords:** artificial nucleoside · deazapurine · Hoogsteen · metal-mediated base pair · Watson–Crick

- [1] a) J. D. Watson, F. H. C. Crick, *Nature* **1953**, *171*, 737–738; b) K. Hoogsteen, *Acta Crystallogr.* **1963**, *16*, 907–916.
- [2] E. N. Nikolova, E. Kim, A. A. Wise, P. J. O'Brien, I. Andricioaei, H. M. Al-Hashimi, *Nature* **2011**, *470*, 498–502.
- [3] a) S. Mandal, A. Hepp, J. Müller, *Dalton Trans.* **2015**, *44*, 3540–3543; b) S. Mandal, M. Hebenbrock, J. Müller, *Angew. Chem. Int. Ed.* **2016**, *55*, 15520–15523; *Angew. Chem.* **2016**, *128*, 15747–15750; c) S. Mandal, C. Wang, R. K. Prajapati, J. Kösters, S. Verma, L. Chi, J. Müller, *Inorg. Chem.* **2016**, *55*, 7041–7050; d) S. Mandal, M. Hebenbrock, J. Müller, *Chem. Eur. J.* **2017**, *23*, 5962–5965; e) S. Mandal, M. Hebenbrock, J. Müller, *Inorg. Chim. Acta* **2018**, *472*, 229–233; f) I. Sinha, C. Fonseca Guerra, J. Müller, *Angew. Chem. Int. Ed.* **2015**, *54*, 3603–3606; *Angew. Chem.* **2015**, *127*, 3674–3677.
- [4] a) S. A. Benner, *Acc. Chem. Res.* **2004**, *37*, 784–797; b) E. Ereemeeva, P. Herdewijn, *Curr. Opin. Biotechnol.* **2019**, *57*, 25–33.
- [5] D. A. Malyshev, F. E. Romesberg, *Angew. Chem. Int. Ed.* **2015**, *54*, 11930–11944; *Angew. Chem.* **2015**, *127*, 12098–12113.
- [6] S. Naskar, R. Guha, J. Müller, *Angew. Chem. Int. Ed.* **2020**, *59*, 1397–1406; *Angew. Chem.* **2020**, *132*, 1413–1423.
- [7] a) B. Jash, J. Müller, *Chem. Eur. J.* **2017**, *23*, 17166–17178; b) Y. Takezawa, J. Müller, M. Shionoya, *Chem. Lett.* **2017**, *46*, 622–633; c) Y. Tanaka, J. Kondo, V. Sychrovský, J. Šebera, T. Dairaku, H. Saneyoshi, H. Urata, H. Torigoe, A. Ono, *Chem. Commun.* **2015**, *51*, 17343–17360; d) J. Müller, *Coord. Chem. Rev.* **2019**, *393*, 37–47.
- [8] Y. Takezawa, M. Shionoya, J. Müller in *Comprehensive Supramolecular Chemistry II, Vol. 4* (Ed.: J. L. Atwood), Elsevier, Oxford, **2017**, pp. 259–293.
- [9] a) T. Nakama, Y. Takezawa, D. Sasaki, M. Shionoya, *J. Am. Chem. Soc.* **2020**, *142*, 10153–10162; b) Y. Takezawa, T. Nakama, M. Shionoya, *J. Am. Chem. Soc.* **2019**, *141*, 19342–19350; c) Y. Takezawa, S. Yoneda, J.-L. H. A. Duprey, T. Nakama, M. Shionoya, *Chem. Sci.* **2016**, *7*, 3006–3010; d) Y. Takezawa, K. Nishiyama, T. Mashima, M. Katahira, M. Shionoya, *Chem. Eur. J.* **2015**, *21*, 14713–14716.
- [10] a) A. Ono, H. Togashi, *Angew. Chem. Int. Ed.* **2004**, *43*, 4300–4302; *Angew. Chem.* **2004**, *116*, 4400–4402; b) B. Jash, P. Scharf, N. Sandmann, C. Fonseca Guerra, D. A. Megger, J. Müller, *Chem. Sci.* **2017**, *8*, 1337–1343; c) B. Jash, J. Müller, *Eur. J. Inorg. Chem.* **2017**, 3857–3861; d) S. Taherpour, O. Golubev, T. Lönnberg, *Inorg. Chim. Acta* **2016**, *452*, 43–49.
- [11] a) S. Hensel, K. Eckey, P. Scharf, N. Megger, U. Karst, J. Müller, *Chem. Eur. J.* **2017**, *23*, 10244–10248; b) J. C. Léon, Z. She, A. Kamal, M. H. Shamsi, J. Müller, H.-B. Kraatz, *Angew. Chem. Int. Ed.* **2017**, *56*, 6098–6102; *Angew. Chem.* **2017**, *129*, 6194–6198; c) T. Ehrenschwender, W. Schmucker, C. Wellner, T. Augenstein, P. Carl, J. Harmer, F. Breher, H.-A. Wagenknecht, *Chem. Eur. J.* **2013**, *19*, 12547–12552; d) S. Liu, G. H. Clever, Y. Takezawa, M. Kaneko, K. Tanaka, X. Guo, M. Shionoya, *Angew. Chem. Int. Ed.* **2011**, *50*, 8886–8890; *Angew. Chem.* **2011**, *123*, 9048–9052.
- [12] J. C. Léon, G. González-Abradelo, C. A. Strassert, J. Müller, *Chem. Eur. J.* **2018**, *24*, 8320–8324.
- [13] a) A. Ono, H. Kanazawa, H. Ito, M. Goto, K. Nakamura, H. Saneyoshi, J. Kondo, *Angew. Chem. Int. Ed.* **2019**, *58*, 16835–16838; *Angew. Chem.* **2019**, *131*, 16991–16994; b) J. Kondo, Y. Tada, T. Dairaku, Y. Hattori, H. Saneyoshi, A. Ono, Y. Tanaka, *Nat. Chem.* **2017**, *9*, 956–960; c) T. Dairaku, K. Furuita, H. Sato, Y. Kondo, C. Kojima, A. Ono, Y. Tanaka, *Nucleosides Nucleotides Nucleic Acids* **2015**, *34*, 877–900; d) S. Katz, *Biochim. Biophys. Acta* **1963**, *68*, 240–253.
- [14] a) S. Johannsen, N. Megger, D. Böhme, R. K. O. Sigel, J. Müller, *Nat. Chem.* **2010**, *2*, 229–234; b) H. Räisälä, T. Lönnberg, *Chem. Eur. J.* **2019**, *25*, 4751–4756; c) D. Ukale, V. S. Shinde, T. Lönnberg, *Chem. Eur. J.* **2016**, *22*, 7917–7923.
- [15] a) H. Weizman, Y. Tor, *J. Am. Chem. Soc.* **2001**, *123*, 3375–3376; b) S. K. Maity, T. Lönnberg, *Chem. Eur. J.* **2018**, *24*, 1274–1277; c) K. Tanaka, A. Tengeji, T. Kato, N. Toyama, M. Shionoya, *Science* **2003**, *299*, 1212–1213.
- [16] a) B. D. Heuberger, D. Shin, C. Switzer, *Org. Lett.* **2008**, *10*, 1091–1094; b) N. Zimmermann, E. Meggers, P. G. Schultz, *Bioorg. Chem.* **2005**, *32*, 13–25.
- [17] G. H. Clever, T. Carell, *Angew. Chem. Int. Ed.* **2007**, *46*, 250–253; *Angew. Chem.* **2007**, *119*, 254–257.
- [18] A. Fujii, O. Nakagawa, Y. Kishimoto, T. Okuda, Y. Nakatsuji, N. Nozaki, Y. Kasahara, S. Obika, *Chem. Eur. J.* **2019**, *25*, 7443–7448.
- [19] a) E.-K. Kim, C. Switzer, *Org. Lett.* **2014**, *16*, 4059–4061; b) E.-K. Kim, C. Switzer, *ChemBioChem* **2013**, *14*, 2403–2407; c) C. Switzer, S. Sinha, P. H. Kim, B. D. Heuberger, *Angew. Chem. Int. Ed.* **2005**, *44*, 1529–1532; *Angew. Chem.* **2005**, *117*, 1553–1556; d) S. Taherpour, O. Golubev, T. Lönnberg, *J. Org. Chem.* **2014**, *79*, 8990–8999; e) S. Taherpour, H. Lönnberg, T. Lönnberg, *Org. Biomol. Chem.* **2013**, *11*, 991–1000; f) J. C. Léon, I. Sinha, J. Müller, *Int. J. Mol. Sci.* **2016**, *17*, 554; g) I. Sinha, J. Kösters, A. Hepp, J. Müller, *Dalton Trans.* **2013**, *42*, 16080–16089.
- [20] a) J. M. Méndez-Arriaga, C. R. Maldonado, J. A. Dobado, M. A. Galindo, *Chem. Eur. J.* **2018**, *24*, 4583–4589; b) N. Santamaría-Díaz, J. M. Méndez-Arriaga, J. M. Salas, M. A. Galindo, *Angew. Chem. Int. Ed.* **2016**, *55*, 6170–6174; *Angew. Chem.* **2016**, *128*, 6278–6282; c) X. Zhou, D. Kondhare, P. Leonard, F. Seela, *Chem. Eur. J.* **2019**, *25*, 10408–10419; d) X. Guo, P. Leonard, S. A. Ingale, J. Liu, H. Mei, M. Sieg, F. Seela, *Chem. Eur. J.* **2018**, *24*, 8883–8892; e) H. Zhao, P. Leonard, X. Guo, H. Yang, F. Seela, *Chem. Eur. J.* **2017**, *23*, 5529–5540; f) H. Yang, F. Seela, *Chem. Eur. J.* **2016**, *22*, 13336–13346.
- [21] I. Sinha, A. Hepp, J. Kösters, J. Müller, *J. Inorg. Biochem.* **2015**, *153*, 355–360.
- [22] B. Lippert, *Coord. Chem. Rev.* **2000**, *200*, 487–516.
- [23] J. Müller, D. Böhme, P. Lax, M. Morell Cerdà, M. Roitzsch, *Chem. Eur. J.* **2005**, *11*, 6246–6253.
- [24] F. Seela, H. Thomas, *Helv. Chim. Acta* **1995**, *78*, 94–108.
- [25] D. A. Megger, C. Fonseca Guerra, J. Hoffmann, B. Brutschy, F. M. Bickelhaupt, J. Müller, *Chem. Eur. J.* **2011**, *17*, 6533–6544.

Manuscript received: June 10, 2020

Accepted manuscript online: July 6, 2020

Version of record online: October 29, 2020